SCIENTIFIC REPORTS
nature research

OPEN

Enhanced Surface Plasmon Resonance Wavelength Shifts by Molecular Electronic Absorption in Far- and Deep-Ultraviolet Regions

Ichiro Tanabe[1]✉, Yoshito Y. Tanaka[2]✉, Koji Watari[3], Wataru Inami[4], Yoshimasa Kawata[4] & Yukihiro Ozaki[3]

In this study, surface plasmon resonance (SPR) wavelength shifts due to molecular electronic absorptions in the far-ultraviolet (FUV, < 200 nm) and deep-ultraviolet (DUV, < 300 nm) regions were investigated by attenuated total reflectance (ATR) spectroscopy. Due to the strong absorption in the DUV region, *N*,*N*-dimethylformamide (DMF) significantly increased the SPR wavelength shift of Al film. On the other hand, no such shift enhancement was observed in the visible region for Au film because DMF does not have absorbance compared to non-absorbing materials such as water and alcohols. The enhanced SPR wavelength shift, caused by the overlap between SPR and molecular resonance wavelengths in FUV-DUV region, is expected to result in high sensitivity for resonant materials.

Recently, surface plasmon resonance (SPR) and localized SPR (LSPR) in the ultraviolet (UV) region have attracted much attention because of higher energy and more abundant electronic transitions in comparison with visible regions[1–14]. For the UV-SPR investigations, Al is a suitable metal because its plasma frequency ($2.4 \times 10^{16}\,s^{-1}$) is higher than the light frequency in the UV regions[15]. The low cost and natural abundance of Al are also its attractive points. For example, fluorescence enhancement and its imaging of biomolecules and cells using Al were reported[4,5]. In the case of surface-enhanced Raman scattering (SERS) in the UV region, the excitation wavelength was down to 229 nm[6–8]. By using the UV light, resonance effect of various molecules such as nucleobases could be utilized. For other instances, photoelectron emission enhancement[9,10], tip-enhanced Raman scattering (TERS)[11,12], and photocatalysis enhancement[13,14] were investigated by using the UV light and Al.

An SPR sensor, which detects refractive index changes near the surface of a metal film, is one of the most important and typical SPR-based applications and is widely used in biochemistry and environmental chemistry[16–20]. Au films are often adopted in commercial SPR sensors, and the Au-based sensors use the lights in the visible region. In contrast, we have recently proposed novel SPR sensors utilizing shorter-wavelength radiation, particularly those in far-ultraviolet (FUV, < 200 nm) and deep-ultraviolet (DUV, < 300 nm) regions[21–23]. While many SPR sensor targets such as proteins and nucleobases have no absorbance in the visible region, they show characteristic and strong absorptions in the FUV-DUV region[24,25]. Some materials such as saccharides absorb light only in the FUV region[26]. Although Al LSPR–based refractive index sensors have been recently reported[27–31], the sensors worked not in the DUV region but in the longer wavelength region, where target molecules have no absorbance. Thus, there is no report about interactions between SPR and molecular electronic transitions in the refractive index sensing in the DUV region.

We have recently reported that the SPR wavelength of an Al film coated on a sapphire prism remained in the DUV region and that the Al films worked as a refractive index sensor even in liquids[21]. In order to investigate the SPR properties in the FUV-DUV regions, our original attenuated total reflectance (ATR) spectrometer was used. Although the SPR properties of Al films in the FUV region have been studied since the 1970's[32–34], their dependence on the refractive index and FUV-DUV-SPR sensor operation have not been described yet. This is because

[1]Graduate School of Engineering Science, Osaka University, Machikaneyama 1-3, Toyonaka, Osaka, 6508531, Japan. [2]Institute of Industrial Science, the University of Tokyo, 4-6-1 Komaba, Meguro, Tokyo, 1538505, Japan. [3]School of Science and Technology, Kwansei Gakuin University, Gakuen 2-1, Sanda, Hyogo, 6691337, Japan. [4]Research Institute of Electronics, Shizuoka University, 3-5-1 Johoku, Hamamatsu, Shizuoka, 4328561, Japan. ✉e-mail: itanabe@chem.es.osaka-u.ac.jp; yoshito@iis.u-tokyo.ac.jp

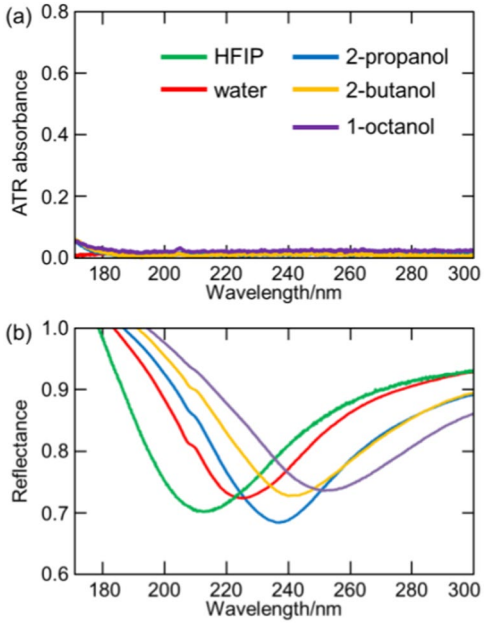

Figure 1. (**a**) Absorption spectra of HFIP, water, 2-propanol, 2-butanol, and 1-octanol. (**b**) Reflection spectra of Al films in the above liquids.

even O_2 and H_2O molecules strongly absorbed light in the FUV region and the investigations had to be performed in a high vacuum atmosphere[32–34]. On the other hand, an ATR prism separates the optics part and the sample part[35,36]. While the optics part is purged with dry N_2 gas, which does not absorb the FUV light, the sample part is exposed to air. Thus, the atmosphere on the Al film can be controlled. Using this technique, SPR wavelengths of Al film on sapphire and quartz prisms were measured. The SPR wavelength shifted to the longer wavelength with the increase of the refractive index *n* on the Al film. Additionally, the effects of Al film thickness were also investigated[22]. However, effects of absorbance of target molecules in the FUV-DUV region was not investigated.

In the present study, the effects of molecular electronic absorptions on SPR sensing were probed by casting liquid samples (1,1,1,3,3,3-hexafluoro-2-propanol (HFIP), water, 2-propanol, 2-butanol, 1-octanol, *N*,*N*-dimethylformamide (DMF), and HFIP/DMF mixtures) on an Al film deposited on a sapphire prism. Importantly, DMF showed a strong absorption peak at ~200 nm, whereas other analytes did not have absorbance in the utilized wavelength range (170–300 nm). As a result, it was revealed that, due to the strong electronic absorptions of DMF (i.e., anomalous dispersion of the refractive index *n*) near the SPR wavelength, the SPR shift was significantly enhanced compared to the other samples which had no absorbance. Such enhancements were not induced in the Au-based visible-SPR sensor. These results indicate that the selection of a specific light absorption wavelength of the target material allows its selective detection due to the marked changes of *n*, which is the advantage the FUV-DUV-SPR sensor.

Results and discussion

Al-SPR wavelength shifts in the presence of liquids without absorbance. The refractive index *n* of the environment close to the Al film surface was tuned by casting of HFIP, water, 2-propanol, 2-butanol, and 1-octanol one by one ($n_D = 1.275$, 1.333, 1.374, 1.396, and 1.428 at 589.3 nm, respectively). The values of n_D present the refractive indices measured at 589.3 nm. ATR absorbance was defined as $-\log(I/I_0)$, where I and I_0 are the reflected light intensities obtained in the presence and absence of a given sample on the sapphire prism, respectively. Figure 1a shows the ATR absorption spectra of these liquid samples. As already mentioned, the above liquids did not have absorbance in the measured wavelength range.

Figure 1b shows the reflection spectra of Al films in HFIP, water, 2-propanol, 2-butanol, and 1-octanol. Reflectance was defined as I_{sample}/I_{air}, where I_{sample} and I_{air} are the intensities of light reflected from the Al film with and without samples, respectively, i.e., the reflectance spectrum measured in air was used as a reference. As discussed previously[23], the Al film/sapphire prism/air system did not exhibit any SPR absorbance and featured an almost constant reflectance intensity in the 170–300 nm range at an incident angle of 70°. Therefore, the reflection spectrum in air could be used as a reference to determine the SPR wavelengths of Al film on which samples were deposited. The SPR wavelengths of the Al in the presence of HFIP, water, 2-propanol, 2-butanol, and 1-octanol were 215.2, 227.5, 238.8, 242.3, and 253.6 nm, respectively. Notably, the sample refractive index *n* and the SPR wavelength were positively correlated.

The SPR wavelength shift induced by changing of *n* on the Al film was simulated using the Fresnel equation as discussed in Appendix A. The effects of Al film oxidation was also discussed in Appendix A. The minimum reflectance was not equal to zero (~0.7; Fig. 1b), which was ascribed to the fact that whereas the utilized incident light comprises both *p*- and *s*-polarized components, only *p*-polarized light can trigger SPR. However, the space constraints of the present system made it difficult to set a polarizer for the FUV-DUV region.

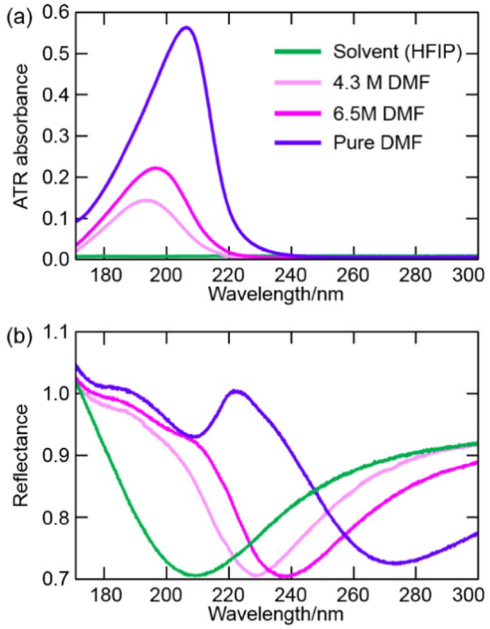

Figure 2. (**a**) ATR absorption spectra of DMF and its mixtures with HFIP. (**b**) Reflection spectra of Al films in the above liquids.

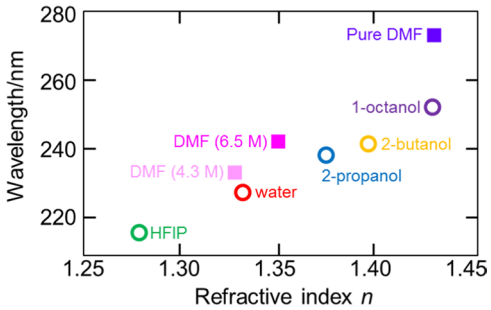

Figure 3. Al-SPR wavelength dependence on the refractive index *n* at 589.3 nm of the samples (open circles) without or (filled squares) with absorbance in the measured wavelength range (170–300 nm).

Al-SPR wavelength shifts in the presence of liquids with absorbance. Subsequently, to investigate the effects of material absorbance (i.e., the extinction coefficient *k* and the anomalous dispersion of *n*), DMF and DMF/HFIP mixtures were cast on Al films. The ATR absorbance spectra of HFIP (as solvent), DMF, and DMF/HFIP mixtures are shown in Fig. 2a. In contrast to the liquid samples in Fig. 1a, DMF had a strong absorbance around 200 nm. Because of the influence of the refractive index *n* of the samples, the ATR spectral shapes around the peak wavelength were distorted depending on the DMF concentration. For 4.3 M, 6.5 M, and pure (13.0 M) DMF, the values of n_D measured by a refractive index sensor (PAL-RI, Atago Co.) equalled 1.328, 1.350, and 1.429, respectively.

These DMF solutions were put on Al films, and reflection spectra were measured. As shown in Fig. 2b, the SPR wavelength increased with increasing DMF concentration (i.e., with increasing *n*). The SPR wavelengths were 215.2, 233.5, 243.0, and 275.6 nm for HFIP, 4.3 M DMF, 6.5 M DMF, and pure DMF, respectively. The reflection dip due to the absorbance of DMF was also observed around 210 nm in the reflection spectrum using pure DMF (Fig. 2b, purple line), which was not affected by the environmental changes.

Figure 3 shows the relationship between *n* and SPR wavelength, with open circles and filled squares being based on the data in Figs. 1b and 2b, respectively.

It should be emphasized here that the refractive index *n* in Fig. 3 was measured at 589.3 nm, which is the wavelength of the sodium D line, and all samples including DMF did not have absorbance in the visible region. As noted above, DMF exhibited a strong absorbance around 200 nm, while other samples had no absorbance in the utilized wavelength range. Since *n* was subject to significant variation around the absorption wavelength (which is denoted as an anomalous dispersion of the refractive index), the use of light with a wavelength close to this value was expected to induce a large SPR wavelength shift. Actually, as shown in Fig. 3, DMF solutions induced a larger shift than water and alcohols, which should result in increased SPR sensor sensitivity. Thus, if the absorption wavelength of DMF is employed, the Al SPR sensor should detect DMF in preference to other materials,

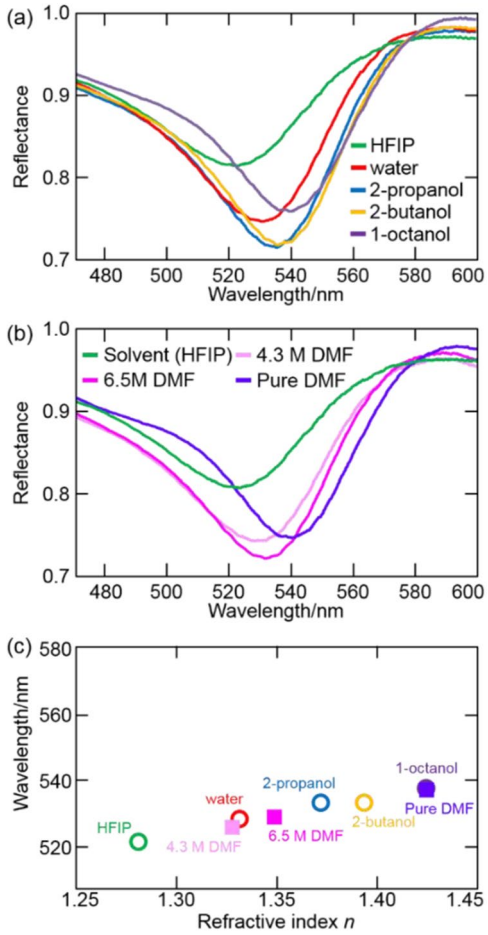

Figure 4. (**a, b**) Au film/sapphire prism reflection spectra in (**a**) HFIP, water, 2-propanol, 2-butanol, 1-octanol, and (**b**) DMF/HFIP mixtures. (**c**) Dependence of Au SPR wavelength on the *n* values (589.3 nm) of different samples.

illustrating the possibility of using FUV-DUV-SPR sensors for highly sensitive and selective analysis. Further quantitative details regarding SPR sensor performance are provided in the Supporting Information (Appendix B).

Au-SPR wavelength shifts in the visible region. Next to that, in order to demonstrate the advantages of the developed FUV-DUV-SPR system as a sensor, we compared it with a common Au film/sapphire prism-based SPR sensor operating in the visible region. As ascribed above, the Au-based SPR sensor is widely used in various fields. Figure 4a and b show the obtained reflection spectra, and Fig. 4c summarizes the dependence of the Au SPR wavelength on *n*.

As for the Al film in the FUV-DUV region, *n* was positively correlated with the Au SPR wavelength, which equalled 523.9, 530.9, 536.0, 536.0, 540.6, 528.3, 531.5, and 539.9 nm for HFIP, water, 2-propanol, 2-butanol, 1-octanol, 4.3 M DMF, 6.5 M DMF, and pure DMF, respectively. However, contrary to the case of the Al film, DMF did not induce a marked Au SPR wavelength shift (Fig. 4c) because DMF also had no absorbance (i.e., no rapid change of *n*) in the visible region, similarly to other samples. Further details regarding the performance of the visible-light SPR sensor are provided in the Supporting Information (Appendix C).

Conclusions

In summary, the effect of the molecular electronic absorption on the SPR wavelength shift was investigated in the FUV-DUV region. Due to the overlap between the SPR wavelength of the Al film and the absorption wavelength of DMF, the SPR shift was enhanced compared to non-resonant materials such as water and alcohols. Such enhancement was not observed for the Au-based visible-SPR sensor because DMF had no absorbance in the visible region. These results indicate that the resonant molecules can be detected sensitively. Many target molecules of the SPR sensor such as nucleotides and proteins have strong absorbance in the FUV-DUV region, and thus, the present FUV-DUV-SPR sensor will lead to the development of novel SPR sensors.

Methods

The Kretschmann configuration was used to excite the SPR of an Al film deposited on a sapphire prism (purchased from Opto-line, Tokyo) by vapour deposition (5.0×10^{-4} Pa, deposition rate ~10 nm s^{-1}). The thickness and surface roughness of the above film were determined as 23.0 ± 0.5 nm by atomic force microscopy.

The prepared Al film was set in on the ATR spectrometer, and reflection spectra were recorded at an incident angle of 70° in the range of 170–300 nm. In order to change the environment close to the Al film surface, HFIP, water, 2-propanol, 2-butanol, 1-octanol, DMF, and HFIP/DMF mixtures were cast on the Al film. We performed simulations based on the Fresnel equations using a bilayer (aluminium and alumina) model to analyse the experimentally obtained spectra.

In order to compare the FUV-DUV-SPR sensor with the visible-SPR sensor, SPR wavelengths of Au films in the visible region were investigated. To acquire visible-region reflection spectra using the same instrument as that used for the FUV-DUV region, the light source was replaced from a deuterium lamp to a Xenon lamp, and the diffraction grating was exchanged to that suitable for the visible region. The measured wavelength range was from 470 to 600 nm. Au films with an optimized thickness (~35 nm) were deposited on the sapphire prism (5.0×10^{-4} Pa, ~1 nm s^{-1}), and the analyte-induced SPR wavelength shifts were investigated.

Received: 26 March 2020; Accepted: 5 May 2020;
Published online: 18 June 2020

References

1. Knight, M. W. *et al*. Aluminum Plasmonic Nanoantennas. *Nano Lett.* **12**, 6000–6004 (2012).
2. Maidecchi, G. *et al*. Deep Ultraviolet Plasmon Resonance in Aluminum Nanoparticle Arrays. *ACS Nano* **7**, 5834–5841 (2013).
3. Bisio, F. *et al*. Pushing the High-Energy Limit of Plasmonics. *ACS Nano* **8**, 9239–9247 (2014).
4. Jiao, X. J., Wang, Y. S. & Blair, S. UV fluorescence enhancement by Al and Mg nanoapertures. *J. Phys. D: Appl. Phys.* **48**, 184007 (2015).
5. Kikawada, M., Ono, A., Inami, W. & Kawata, Y. Plasmon-Enhanced Autofluorescence Imaging of Organelles in Label-Free Cells by Deep-Ultraviolet Excitation. *Anal. Chem.* **88**, 1407–1411 (2016).
6. Dorfer, T., Schmitt, M. & Popp, J. Deep-UV surface-enhanced Raman scattering. *J. Raman Spectrosc.* **38**, 1379–1382 (2007).
7. Jha, S. K., Ahmed, Z., Agio, M., Ekinci, Y. & Loffler, J. F. Deep-UV Surface-Enhanced Resonance Raman Scattering of Adenine on Aluminum Nanoparticle Arrays. *J. Am. Chem. Soc.* **134**, 1966–1969 (2012).
8. Sharma, B. *et al*. Aluminum Film-Over-Nanosphere Substrates for Deep-UV Surface-Enhanced Resonance Raman Spectroscopy. *Nano Lett.* **16**, 7968–7973 (2016).
9. Malicka, J., Gryczynski, I., Gryczynski, Z. & Lakowicz, J. R. Surface plasmon-coupled ultraviolet emission of 2,5-diphenyl-1,3,4-oxadiazole. *J. Phys. Chem. B* **108**, 19114–19118 (2004).
10. Watanabe, Y., Inami, W. & Kawata, Y. Deep-ultraviolet light excites surface plasmon for the enhancement of photoelectron emission. *J. Appl. Phys.* **109**, 023112 (2011).
11. Sands, H. S. *et al*. Development of a combined confocal and scanning near-field Raman microscope for deep UV laser excitation. *J. Raman Spectrosc.* **33**, 730–739 (2002).
12. Taguchi, A., Hayazawa, N., Furusawa, K., Ishitobi, H. & Kawata, S. Deep-UV tip-enhanced Raman scattering. *J. Raman Spectrosc.* **40**, 1324–1330 (2009).
13. Honda, M., Kumamoto, Y., Taguchi, A., Saito, Y. & Kawata, S. Plasmon-enhanced UV photocatalysis. *Appl. Phys. Lett.* **104**, 061108 (2014).
14. Honda, M., Kumamoto, Y., Taguchi, A., Saito, Y. & Kawata, S. Efficient UV photocatalysis assisted by densely distributed aluminum nanoparticles. *J. Phys. D: Appl. Phys.* **48**, 184006 (2015).
15. Ehrenreich, H., Philipp, H. R. & Segall, B. Optical properties of aluminum. *Phys. Rev.* **132**, 1918–1928 (1963).
16. Liedberg, B., Nylander, C. & Lundstrom, I. Surface-Plasmon Resonance for Gas-Detection and Biosensing. *Sens. Actuators* **4**, 299–304 (1983).
17. Homola, J. Present and future of surface plasmon resonance biosensors. *Anal. Bioanal. Chem.* **377**, 528–539 (2003).
18. Homola, J. Surface plasmon resonance sensors for detection of chemical and biological species. *Chem. Rev.* **108**, 462–493 (2008).
19. Masson, J. F. Surface Plasmon Resonance Clinical Biosensors for Medical Diagnostics. *ACS Sens.* **2**, 16–30 (2017).
20. Hinman, S. S., McKeating, K. S. & Cheng, Q. Surface Plasmon Resonance: Material and Interface Design for Universal Accessibility. *Anal. Chem.* **90**, 19–39 (2018).
21. Tanabe, I. *et al*. Far- and deep-ultraviolet surface plasmon resonance sensors working in aqueous solutions using aluminum thin films. *Sci. Rep.* **7**, 5934 (2017).
22. Tanabe, I. *et al*. Aluminum Film Thickness Dependence of Surface Plasmon Resonance in the Far- and Deep-ultraviolet Regions. *Chem. Lett.* **46**, 1560–1563 (2017).
23. Tanabe, I. *et al*. Direct optical measurements of far- and deep-ultraviolet surface plasmon resonance with different refractive indices. *Opt. Express* **24**, 21886–21896 (2016).
24. Fodor, S. P. A., Rava, R. P., Hays, T. R. & Spiro, T. G. Ultraviolet Resonance Raman-Spectroscopy of the Nucleotides with 266-nm, 240-nm, 218-nm, and 200-nm Pulsed Laser Excitation. *J. Am. Chem. Soc.* **107**, 1520–1529 (1985).
25. Goto, T., Ikehata, A., Morisawa, Y. & Ozaki, Y. Electronic Transitions of Protonated and Deprotonated Amino Acids in Aqueous Solution in the Region 145-300 nm Studied by Attenuated Total Reflection Far-Ultraviolet Spectroscopy. *J. Phys. Chem. A* **117**, 2517–2528 (2013).
26. Uchiho, Y. *et al*. Far-ultraviolet absorbance detection of sugars and peptides by high-performance liquid chromatography. *J. Chromatogr. A* **1424**, 86–91 (2015).
27. Chan, G. H., Zhao, J., Schatz, G. C. & Van Duyne, R. P. Localized surface plasmon resonance spectroscopy of triangular aluminum nanoparticles. *J. Phys. Chem. C* **112**, 13958–13963 (2008).
28. Norek, M., Wlodarski, M. & Matysik, P. UV plasmonic-based sensing properties of aluminum nanoconcave arrays. *Curr. Appl. Phys.* **14**, 1514–1520 (2014).
29. Li, W. B., Zhang, L., Zhou, J. H. & Wu, H. K. Well-designed metal nanostructured arrays for label-free plasmonic biosensing. *J. Mater. Chem. C* **3**, 6479–6492 (2015).
30. Li, W. B. *et al*. Aluminum nanopyramid array with tunable ultraviolet-visible-infrared wavelength plasmon resonances for rapid detection of carbohydrate antigen 199. *Biosens. Bioelectron.* **79**, 500–507 (2016).
31. Couture, M., Ray, K. K., Poirier-Richard, H. P., Crofton, A. & Masson, J. F. 96-Well Plasmonic Sensing with Nanohole Arrays. *ACS Sens.* **1**, 287–294 (2016).
32. Pettit, R. B., Silcox, J. & Vincent, R. Measurement of Surface-Plasmon Dispersion in Oxidized Aluminum Films. *Phys. Rev. B* **11**, 3116–3123 (1975).
33. Callcott, T. A. & Arakawa, E. T. Volume and Surface Photoemission Processes from Plasmon Resonance Fields. *Phys. Rev. B* **11**, 2750–2758 (1975).
34. Higashi, N., Ikehata, A. & Ozaki, Y. An attenuated total reflectance far-UV spectrometer. *Rev. Sci. Instrum.* **78**, 103107 (2007).
35. Ozaki, Y., Morisawa, Y., Ikehata, A. & Higashi, N. Far-Ultraviolet Spectroscopy in the Solid and Liquid States: A Review. *Appl. Spectrosc.* **66**, 1–25 (2012).
36. Ozaki, Y. & Tanabe, I. Far-ultraviolet spectroscopy of solid and liquid states: characteristics, instrumentation, and applications. *Analyst* **141**, 3962–3981 (2016).

Acknowledgements
This work was financially supported by JSPS KAKENHI (Grant No. JP18K14251) and Advanced Technology Institute Research Grants 2017.

Author contributions
I.T. and Y.Y.T. contributed equally to this work. I.T. mainly conducted the present study and prepared the manuscript. Y.Y.T. mainly conceived the present study and prepared the manuscript. K.W. mainly measured and analyzed FUV–DUV spectra. W.I. prepared the Al film. Y.K. and Y.O analyzed and discussed all data in the manuscript. All authors discussed the results and shared the manuscript.

Competing interests
The authors declare no competing interests.

Additional information
Supplementary information is available for this paper at https://doi.org/10.1038/s41598-020-66949-z.

Correspondence and requests for materials should be addressed to I.T. or Y.Y.T.

Reprints and permissions information is available at www.nature.com/reprints.

Publisher's note Springer Nature remains neutral with regard to jurisdictional claims in published maps and institutional affiliations.